IEEE ComSoc IEEE Open Journal of the Communications Society

Received XX Month, XXXX; revised XX Month, XXXX; accepted XX Month, XXXX; Date of publication XX Month, XXXX; date of current version 11 January, 2024.

Digital Object Identifier 10.1109/OJCOMS.2024.011100

C-RAN and Optical Fronthaul Latency in Representative Network Topologies

Dave Townend[1,2], Stuart D. Walker [2], Neil Parkin [1], Anvar Tukmanov [1] *(Senior Member, IEEE)*

[1]BT Laboratories, Adastral Park, Martlesham, U.K
[2]University of Essex, Wivenhoe Park, Colchester, UK

CORRESPONDING AUTHOR: Dave Townend (e-mail: dt19651@essex.ac.uk).

ABSTRACT This paper presents a feasibility study aimed at understanding centralized radio access network (C-RAN) deployments based on incumbent distributed radio access network (D-RAN) topologies. A model is derived to allow realistic latency characteristics to be calculated for fronthaul connectivity between existing cell sites and transport network aggregation nodes (hubs) suitable for baseband centralization. Analysis has demonstrated that as much as 96% of urban cell site neighbor pairs could satisfy C-RAN fronthaul latency budgets if baseband processing were to be centralized at the local transport hub and 91% when centralized at the regional transport hub using single mode fiber. Findings suggest that the feasibility of advanced coordinated transmission schemes between such pairings could be realized based on existing real-world fiber deployment topologies. Furthermore, the proportion of sites that could support C-RAN requirements could be increased further to 97% when aggregated at local transport hubs and 95% at regional hubs where hollow core fiber transport solutions are employed.

INDEX TERMS C-RAN, Centralization, Fronthaul, CoMP, Latency

I. Introduction

AMONGST many objectives under consideration for 6G is the deployment and operational simplification of the radio access network (RAN) [7]. One such concept is the transition towards centralization of the RAN known as C-RAN. Whilst C-RAN has been considered for many years as a more ideal deployment architecture over traditional distributed baseband cell sites, it is only recently that standardization efforts have allowed such deployment architectures to become more practically and economically viable. New 'functional split' transport interfaces defined in 3GPP release 14 [1] outline eight possible interface options in the RAN protocol stack between the traditional baseband unit (BBU) and radio unit. These new specifications enable greater flexibility in how the constituent 5G RAN components, centralized unit (CU), distributed unit (DU) and radio unit (RU) can be deployed.

Through centralizing the DU and CU baseband components at common geographic locations away from the cell site, a range of advanced cell coordination techniques foreseen in 6G can be enabled [3]. This may come is the form of dynamic point selection (DPS) where a single cell site transmission/reception point (TRP) is used but which can be changed dynamically to other TRPs in range, non-coherent joint transmission (NC-JT) where spatial diversity layers from multiple TRPs can be employed without the requirement for phase accurate channel state information (CSI) and coherent joint transmission schemes (C-JT) requiring accurate CSI to compute a beam-forming transmission precoder utilized across multiple TRPs. The associated benefits of these coordination techniques promise reduction or even removal of conventional cell edge interference, enhanced spectral efficiencies in coverage overlap regions and cost efficiencies enabled by heuristic energy saving underpinned by machine learning and artificial intelligence applications [5], [21]. The difficultly in realizing such potential of C-RAN in real networks lie in the fundamental requirements for any such coordinating cells to be both tightly synchronized and connected via low latency fronthaul links to ensure coordinated signaling information remains accurate.

Within the constraints of the fronthaul driven C-RAN deployment come decisions around how and where to place baseband functions within the network topology that could address both the stringent transport requirements and support the clustering of a multitude of localized or regional cell sites. For network operators, this may be a question of which network aggregation sites (i.e. data center or transport network hub site) in the wider network maximize the feasibility

This work is licensed under a Creative Commons Attribution 4.0 License. For more information, see https://creativecommons.org/licenses/by/4.0/

of centralization and consequently unlocks the anticipated benefits of cell coordination. Before any theoretical gains and use cases of C-RAN are explored further, it is important to first consider the feasibility of such architectures in realistic network topologies. Whilst the ideal C-RAN deployment assumes ubiquitous fiber transport connectivity capable of delivering the high capacity low latency fronthaul performance necessary [2], the practical reality is that in many geographies this would still be cost prohibitive at scale. As such, early focus on C-RAN and advanced cell site coordination technologies envisaged for 6G will target high value dense urban areas where coordination gains and the availability of the fiber connectivity necessary are expected to be greatest.

II. Related Work

The benefits of centralization of the RAN baseband have been widely studied particularly from the perspective of coordinated or joint transmissions schemes from multiple cell sites or TRPs towards active users [14]. Such studies have generally been confined to theoretical approaches focused on the relative merits of advanced cooperative transmissions. In [15], dynamic point selection (DPS) and non-coherent joint transmission (NC-JT) are explored where findings suggest NC-JT does not provide performance gains over DPS unless there is a TRP channel that is rank deficient. In [22] analysis also suggests that NC-JT implementations utilizing a distributed scheduling approach may out perform NC-JT using a centralized scheduler due to greater freedom and flexibility in scheduling decisions. Experimental studies of C-JT schemes have been reported in [20] where findings have demonstrated close to theoretical 6dB SNR gain when using analogue radio-over-fiber (RoF) fronthaul links.

From a deployment feasibility perspective, C-RAN or user centric studies generally ignore connectivity requirements or assume an ideal fronthaul capability [22]. Alternatively, fronthaul is often considered constrained and transmission schemes compared or performance of the RAN adjusted to compensate [18]. Other associated studies focus on placement of DU/CU processing capabilities for cell clustering but are typically optimization problems built on stochastic approaches rather than constraints imposed by real network infrastructure deployments [16]. Such theoretical approaches do not typically represent a realistic deployment strategy for C-RAN and as such, there remains literature gaps providing insight into the feasibility and extent to which fronthaul could be applied to real-world deployments as well as where DU/CU centralization nodes could be placed in the existing network topology built around legacy D-RAN architectures.

III. Organisation

The objective of this study is to characterize realistic transport links in order to understand the latency constraints between cell site locations and potential aggregation sites where DU/CU baseband processing could be centralized. In Section IV a detailed topology model is presented where road network data sets are used to estimate fiber optic transport paths and associated fiber lengths between key infrastructure locations in a typical urban environment. In Section V the fundamental latency requirements of fronthaul oriented deployments are discussed which represent the total fronthaul latency budget that must be satisfied for C-RAN cell sites in the model. To support assumptions about latency contributions calculated in the model, experimental results are presented which outline the Ethernet switch port delays and fiber optic propagation delays of a representative fiber transport solution. In Section VI, the results for latency calculations that are able to satisfy the fronthaul latency budget between each combination of neighboring cell sites in the model is presented. Findings demonstrate the proportion of existing cells that could coordinate from a common DU/CU location when homed at the local transport network hub site (1st tier 'exchange' site) or deeper in the network at a regional transport network hub site (2nd tier 'metro' site). A comparison of the use of conventional single mode fiber (SMF) and lower latency hollow core fiber (HCF) is also presented. Conclusion are summarized in Section VII.

IV. Fronthaul Deployment Model

The fronthaul latency characteristics of a dense urban RAN deployment is analyzed using a representative 20 sq km study area of central London, UK. The underlying infrastructure and transport network topology is approximated using public domain data sets as exact infrastructure locations and fiber duct routing is proprietary and commercially sensitive information unpublished by associated infrastructure providers. As such, the fiber routes from existing cell site locations (1090 cell sites) in the model and between (95 local) exchange locations or (8 regional) metro locations are assumed to approximately trace the public road network in a similar vein to other utilities infrastructure. The full fronthaul deployment model is subsequently built up of two sets of transport network topologies; 'access links' representative of fiber links between the customer site (i.e. cell site) and the local exchange site and 'main links' representative of the inter-exchange fiber links as depicted in Fig.1.

A. Access Link Topology Model

The 'access link' paths between existing cell sites and their closest exchange transport hub site are built whereby Voronoi polygons are constructed for each exchange site in the model. Any cell site that lies within the Voronoi boundary are assumed to be served by this closest exchange site and so a shortest path algorithm is used to calculate the fiber route and length via the road network layout. It should be noted that in real deployments operators may often choose to multi-home cell sites to alternative exchange sites for purposes of resiliency and redundancy - a factor which is not considered in this study.

This article has been accepted for publication in IEEE Open Journal of the Communications Society. This is the author's version which has not been fully edited and content may change prior to final publication. Citation information: DOI 10.1109/OJCOMS.2025.3542479

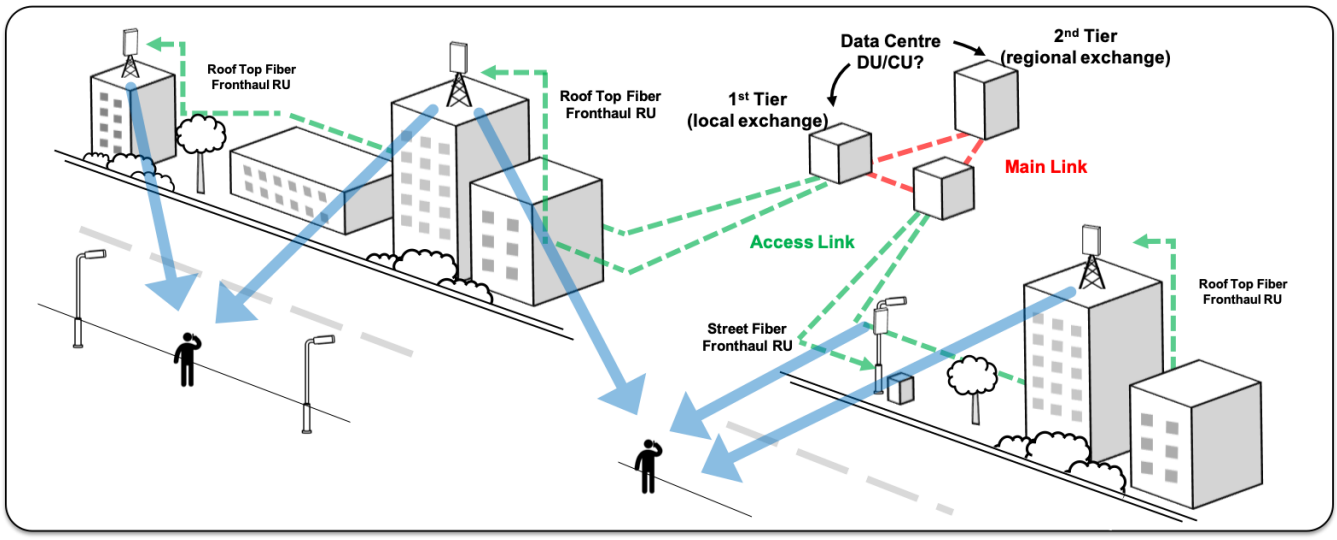

FIGURE 1. **Example C-RAN deployment scenario where the ability to coordinate cell sites using common baseband capabilities is dependent on latency constraints within the fiber optic transport network.**

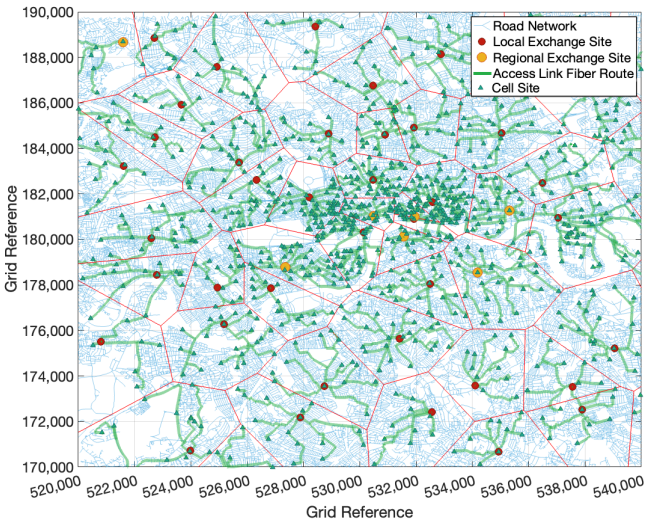

FIGURE 2. **Access link fiber topology model.**

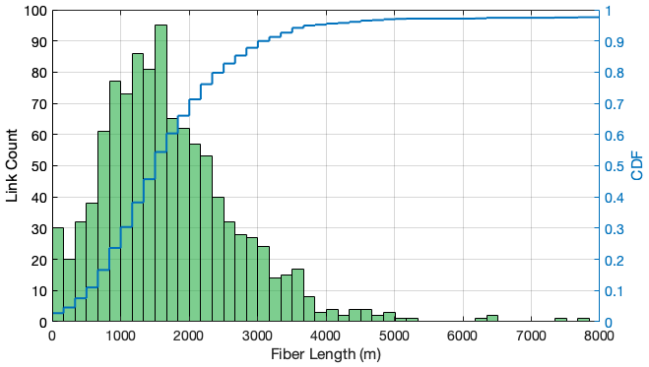

FIGURE 3. **Access link fiber length distribution.**

The resulting fiber transport network topology is given in Fig. 2 and the associated fiber length distribution for all cell sites within the model in Fig. 3. The fiber length distribution represents a realistic distribution for transport access links to cells which terminate their fronthaul connectivity to the 1st available (closest) network aggregation tier suitable for centralization of baseband. In a dense urban deployment covered by the study area the mean fiber length observed was 1740 m between cell site and closet local exchange site.

B. Main Link Topology Model

To complement the access link topology, an equivalent methodology is used to model 'main link' paths within the same environment. The main link paths represent core fiber links assumed to exist between network exchange sites which join neighboring local and regional exchange sites. Again, the road network is used to approximate paths between logical neighbors. The resulting fiber topology is presented in Fig. 4 and the associated fiber length distribution for all inter-exchange links within the model in Fig. 5. The main link routes are necessary to calculate more complicated transport network routes which may require cell sites to coordinate across exchange boundaries or for the scenario where DU/CU baseband is centralized deeper in the network at larger regional exchange sites. The mean fiber length observed between exchange sites in the urban study area was 4736 m.

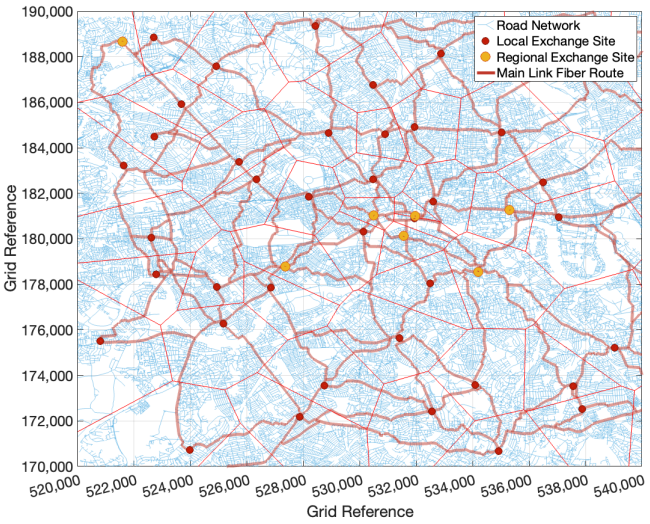

FIGURE 4. **Main link fiber topology model.**

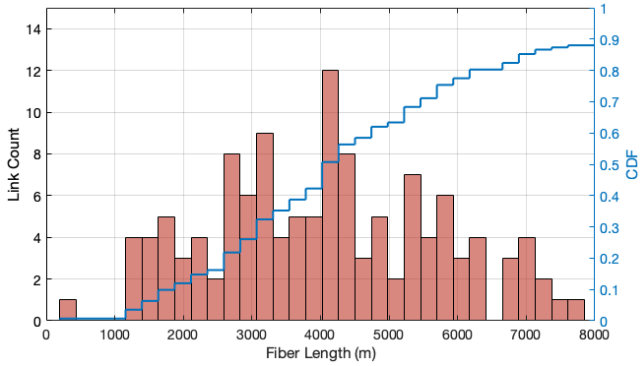

FIGURE 5. **Main link fiber length distribution.**

V. C-RAN Transport

With the transport network route topology and each cell site fiber length characterized, the model can be used to build fronthaul latency budgets necessary to identify which cell sites and cell site pairings could be deployed as C-RAN RU nodes capable of coordinated transmission schemes. In the envisaged deployment, each RU in the model is assumed to be connected using a low layer split interface such as O-RAN 7.2x (3GPP option 7.2) with the associated fronthaul latency performance requirements.

While a variety of WDM (Wavelength Division Multiplexing) and Ethernet multiplexing schemes may be interchangeably considered in the fronthaul architecture [13], the fiber transport technology assumed in this study is DWDM [10] (Dense Wavelength Division Multiplexing) in the C band. The objective is to maximize the fiber channel multiplexing over a single (using bidirectional wavelengths) transport fiber to reduce infrastructure and operational costs whilst maximizing the fiber availability. Other WDM schemes such as Coarse WDM [12] and LAN-WDM [11] could also be used allowing lower cost O band optical interfaces to be used but with a limitation on reach due to the higher attenuation found in SMF fibers in this region.

A. Fronthaul Latency Requirement

Fronthaul transport specifications such as 802.1CM [8], O-RAN [17] and eCPRI [6] define a range of latency classes depending on how the RU may be configured. The permissible fronthaul delay budget can vary between 25 μs for low latency communication use cases to 500 μs for larger latency deployments requiring longer transport propagation delays or switching delay in multi-hop transport networks. For a typical 'Full E-UTRA or NR Performance' cell as assumed in this study, these specifications are aligned with a one-way delay of 100 μs as highlighted in Table 1. Here, it is assumed that legacy 4G LTE radio (constrained by use of fixed synchronous uplink HARQ procedures) would continued to play a role in the envisaged C-RAN migration strategy. It is however recognized that future 5G/6G only deployments with more flexible radio interface configurations could offer new low latency access use cases necessitating use of the more stringent High75/High25 latency classes although these are not addressed in this study.

Any control plane traffic required for scheduling and beamforming precoding generally have a much greater latency tolerance ranging from between 1 ms and 100 ms. As such, the upper limit for latency budget that must be satisfied between each RU and centralized DU located in the model is assumed to be 100 μs.

B. Experimental Ethernet Transport Contributions

The delay contributions required in the model's latency budget are derived from the Ethernet latency characterization of a representative transport solution in lab conditions. The transport solution setup is outlined in Fig. 6 and Fig. 7 where an active high capacity Ethernet switch with uncontended non-blocking ports is assumed at both the cell site, connecting to the RU, and at the centralized site connecting to the DU. It should be noted that this scenario represents the ideal scenario where queuing delay contributions resulting from a mix of latency classes or port congestion are not considered. Between each RU and DU location a DWDM implementation is used to multiplex ports to a single fiber solution across any intermediate access and main link fibers. The DWDM solution utilizes passive filters which contribute only a small amount of fiber propagation delay. The configuration used was unamplified, with the unused amplifier ports bypassed by a fiber loop. The line side optical transceivers were 10 Gb/s using C band wavelengths at 1530.33 nm and 1529.55 nm. An Ethernet tester was connected across the transport solution between the end points to allow accurate latency measurements to be taken for varying lengths of single mode and hollow core fiber (as well as the absence of significant fiber length in the 'back2back' case) as presented in Table. 2. The SMF fiber measured was G.652.D [9] and the HCF fiber was the anti-resonant type with lower refractive index

TABLE 1. Summary of Fronthaul Latency Requirements.

	eCPRI[6]	O-RAN [17]	IEEE [8]	One-way Delay Requirement	4G LTE User Plane	4G LTE Control Plane	5G NR User Plane	5G NR Control Plane	Application
High	High25	High25	Class 2	$25\mu s$			✓		Full NR Ultra-low latency performance
	-	High75	-	$75\mu s$			✓		Full NR performance with fiber lengths in the 10 km range
	High100	High100	Class1/Class2	$100\mu s$	✓		✓		Full E-UTRA or NR performance
	High200	High200	Class2	$200\mu s$			✓		Installations with fiber links lengths in the 40 km range
	High500	High500	Class2	$500\mu s$			✓		Large latency installations
Medium	Medium	Medium	Class2	1ms		✓	✓	✓	User Plane (slow), C and M Plane (fast)
Low	Low	Low	Class2	100ms		✓		✓	C and M Plane (slow)

■ Maximum fronthaul latency requirement T_{RU-DU} = $100\mu s$

as described in previous work [19]. The Ethernet test traffic performance measurements are aligned with RFC 2544 test procedures [4] at 0% frame loss and with a $\pm$ 10 ns accuracy. The constituent delay contributions measured from the switch-port t_{SW} of 16.46 μs and propagation delay coefficients for SMF τ_{SMF} of 4.95 $\mu s/km$ and HCF τ_{HCF} of 3.40 $\mu s/km$ are subsequently used in latency calculations in the topology model.

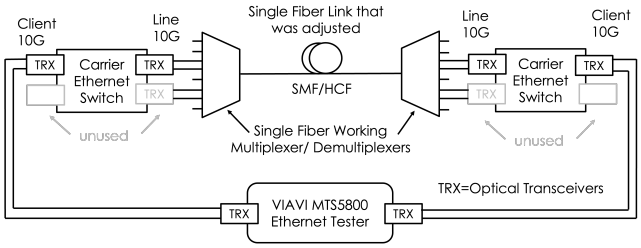

FIGURE 6. Transport network solution measurement configuration.

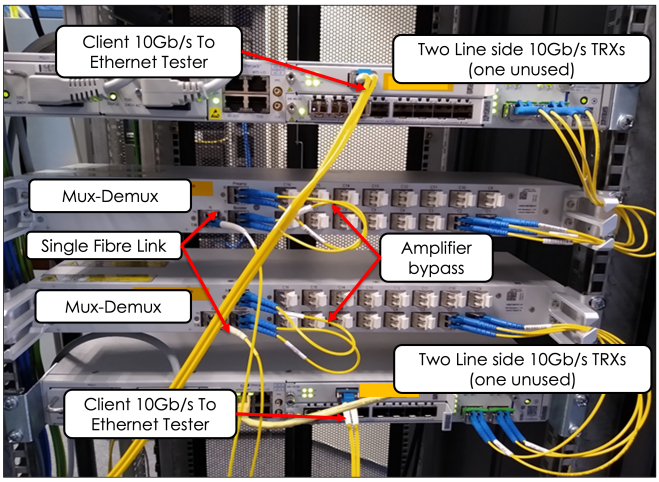

FIGURE 7. Transport network solution latency measurement.

C. Fronthaul System Model

With example requirements identified and latency parameters derived, a system model is defined that incorporates the topology fiber lengths in Section IV and the delay constants from Section V-B. In the envisaged C-RAN architecture the DU and CU are centralized in two different scenarios 1) at the closest local exchange site to each cell site (first tier of the transport network topology) and 2) the subsequent and larger second tier of aggregation at a regional exchange site. In both the scenarios we follow the system model outlined in Fig. 8. The latency delay budget outlined in 1 is used for coordinating cells which share the same local exchange and 2 where coordinating cells may span exchange boundaries (main link fibers) or for the regional exchange aggregation scenario.

To validate each cell site as capable of operating in a C-RAN deployment the total fronthaul latency between RU and DU T_{RU-DU} must be below the 100 μs fronthaul requirement as defined in Section V-A. Passive latency contributions resulting from fiber optic propagation are a product of the propagation delay constant τ of which there values for SMF and HCF, and the total fiber length. In the model, the total fiber length consists of the fiber length of the access link d_{ACCESS} and, in the regional aggregation or cross-boundary scenario, one or more hops over main link fibers d_{MAIN}. In addition, smaller fiber lengths from roadside and indoor runs at the RU $d_{RU_{prem}}$ and DU $d_{DU_{prem}}$ end are accounted for with calculations between the closest road edge and center of the premises geographic location.

$$T_{RU-DU_{local}} = \tau(d_{RU_{prem}} + d_{ACCESS} + d_{DU_{prem}}) + 2t_{SW} \leq 100\mu s \quad (1)$$

$$T_{RU-DU_{regional}} = \tau(d_{RU_{prem}} + d_{ACCESS} + d_{MAIN(i)} + d_{DU_{prem}}) + 2t_{SW} \leq 100\mu s \quad (2)$$

TABLE 2. Summary of Fronthaul Latency Measurements.

	Measured Ethernet Round Trip Delay			Calculated Ethernet One-Way Delay			Fiber Propagation Delay Only	
	Avg (μs)	Min (μs)	Max (μs)	Avg (μs)	Min (μs)	Max(μs)	Avg (μs)	Avg (μs/km)
Back2Back 0 km SMF	32.92	32.69	33.70	16.46	16.35	16.85	-	-
4.1 km SMF	73.60	73.22	74.26	36.80	36.61	37.13	20.34	4.91
6.3 km SMF	96.51	96.29	97.31	48.25	48.15	48.66	31.79	5.05
10 km SMF	131.24	130.86	131.95	65.62	65.43	65.98	49.16	4.90
4.1km HCF	61.08	60.77	61.68	30.54	30.39	30.84	14.08	3.43
6.2 km HCF	74.76	74.44	75.47	37.38	37.22	37.74	20.92	3.37
10.3 km HCF	102.22	101.91	103.03	51.11	50.96	51.52	34.65	3.38

Switchport delay contribution t_{SW} = 16.46 μs

Mean fiber propagation delay constant τ, SMF = 4.95 $\mu s/km$, HCF = 3.40 $\mu s/km$

Active latency contributions are those assumed from Ethernet switch ports in the transport solution t_{SW}. There are many deployment configurations in which active Ethernet components may be deployed, and while it is desirable to remove these where possible it is assumed active fronthaul aggregation switches are utilized only once at each end of the transport link. The anticipated high port density at the DU node necessitates Ethernet aggregation from multiple cell sites while Ethernet switch use at the cell site may be necessary both for operational requirements but also to minimize the cost associated with swap out to DWDM channelized SFPs (Small Form-factor Plugables) at the mast head. As such, where main links are traversed, it is assumed passive fiber patching is used to 'glass-through' from access links to main link fiber chains which do not contribute further active delay contributions to the path.

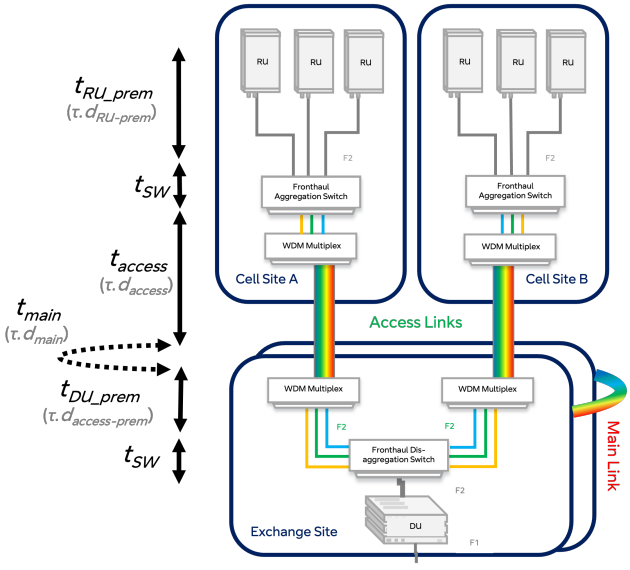

FIGURE 8. System model for fronthaul latency characterization.

Crucially, to coordinate any neighbor sites and unlock the potential of coordinated transmission schemes each coordinating neighbor must both be able to meet this requirement. In order to quantify the feasibility of C-RAN in the representative network topology the latency budget for each combination of neighbor cell pairing is calculated from the topology model. Cell neighbor pairings are constructed by calculating the geometric neighbors of each cell using Delaunay triangulation as shown in Fig. 9. Each unique pairing represents the feasibly of those cells coordinating from common baseband capability. It should be noted that these geometric boundaries/coordination sets in the model do not guarantee regions of coverage overlap in a real network due to specific antenna orientation, transmit power levels and frequencies in use and so such neighbor pairings are considered a best case or upper bound condition.

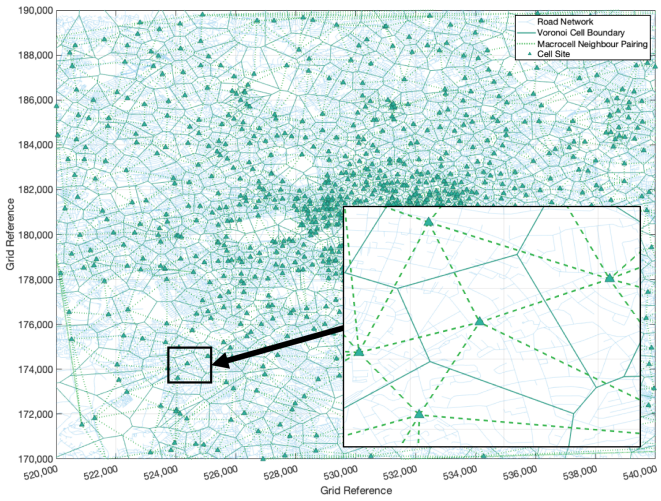

FIGURE 9. Logical cell site neighbors which could coordinate transmissions in areas of coverage overlap.

VI. Fronthaul Deployment Latency Results

For each combination of coordinating cells as outlined in Fig. 9 the end-to-end latency budget is calculated for both scenarios where the DU is homed at the local exchange and the regional exchange. In each scenario the use of single mode fiber and hollow core fiber are compared. The DU homing at the local exchange site is given in Fig. 10 for SMF and Fig. 11 for HCF. Analysis show promising results where 96% of neighbor pairs could satisfy the fronthaul

latency budget and thus enable cell coordination techniques assuming traditional SMF and 97% if HCF is used. The lower propagation delay of HCF has shown only a modest footprint gain in this scenario relative to SMF fronthaul.This is primarily due to the relatively short access fiber lengths observed in the dense urban study area as previously highlighted in Fig. 3. On average, the local exchange site would be required to support DU capacity for 18 cell sites in a dense urban deployment.

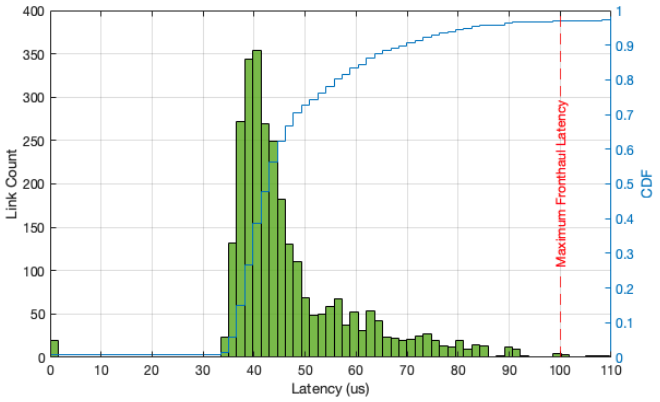

FIGURE 10. Latency distribution of cell pairings homed to local exchange using SMF.

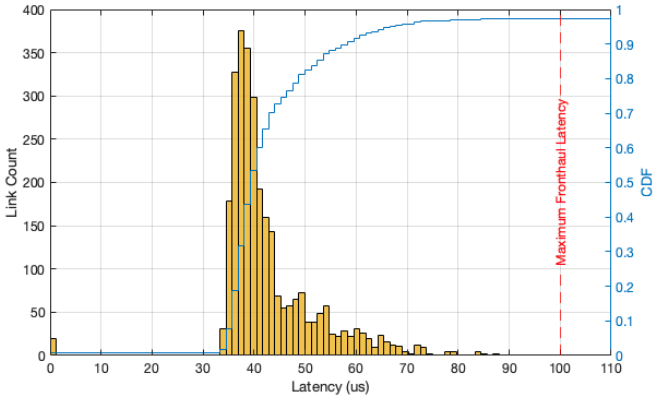

FIGURE 11. Latency distribution of cell pairings homed to local exchange using HCF.

When considering DU aggregation at the regional exchange site, the proportion of viable coordinating neighbor sites does however reduce. The distribution of fronthaul latency in this scenario for SMF and HCF is given in Fig. 12 and Fig. 13 respectively. Here, only 91% of neighbor pairs could feasibility coordinate using conventional SMF, this however, could be extended to as much as 95% if HCF were to be used. The reduction in C-RAN capable cell pairings is primarily a result of the additional main link paths introduced when routing to regional exchange sites. In the example study area, homing of DU capabilities at regional hubs would on average need to support DU capacity for 115 cell sites.

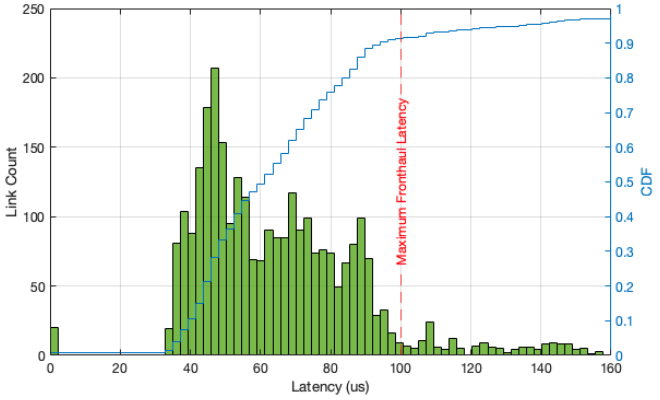

FIGURE 12. Latency distribution of cell pairings homed to regional exchange using SMF.

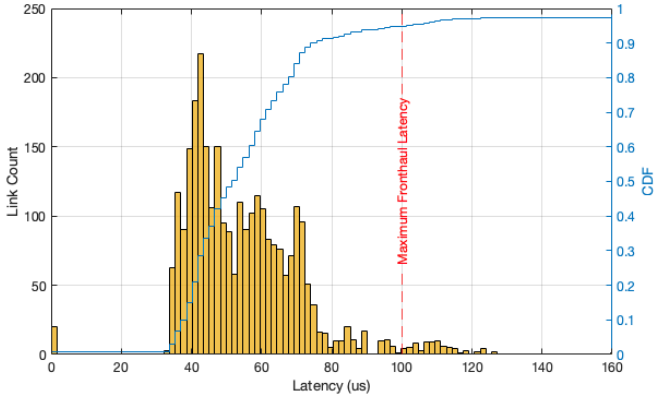

FIGURE 13. Latency distribution of cell pairings homed to regional exchange using HCF.

VII. Conclusions

In this paper we contribute new insights into the deployment feasibility of C-RAN based on representative fiber topologies and the associated implications to fronthaul latency. Findings have shown that a long term migration from conventional backhaul driven distributed cell sites towards a fronthaul based centralized architecture is feasible without fundamental redesign of the underlying transport network. Assuming the use of layer 2 Ethernet hops are minimized, as much as 96% of urban cell sites could be centralized to the first tier or edge estate of the network. Where larger scale centralization is envisaged as much as 91% of sites could be aggregated to regional nodes in the transport network. In addition, the deployment of HCF in fronthaul networks has been shown to significantly expand the achievable footprint of C-RAN. While HCF is not widely deployed in modern networks and any replacement of conventional SMF is likely to be costly, findings do suggest a more strategic approach to use of HCF targeting longer length main links may be sufficient to maximize the viability of C-RAN and fronthaul driven networks whilst minimizing associated cost.

References

[1] 3GPP. *TR 38.801 V14.0.0 Study on new radio access technology: Radio access architecture and interfaces*. 2017.

[2] Isiaka Ajewale Alimi, António Luís Teixeira, and Paulo Pereira Monteiro. "Toward an Efficient C-RAN Optical Fronthaul for the Future Networks: A Tutorial on Technologies, Requirements, Challenges, and Solutions". In: *IEEE Communications Surveys and Tutorials* 20.1 (2018), pp. 708–769. DOI: 10.1109/COMST.2017.2773462.

[3] Hussein A. Ammar et al. "User-Centric Cell-Free Massive MIMO Networks: A Survey of Opportunities, Challenges and Solutions". In: *IEEE Communications Surveys and Tutorials* 24.1 (2022), pp. 611–652. DOI: 10.1109/COMST.2021.3135119.

[4] *Benchmarking Methodology for Network Interconnect Devices*. RFC 2544. Mar. 1999. DOI: 10.17487/RFC2544. URL: https://www.rfc-editor.org/info/rfc2544.

[5] Jiacheng Chen et al. "Evolution of RAN Architectures Toward 6G: Motivation, Development, and Enabling Technologies". In: *IEEE Communications Surveys and Tutorials* 26.3 (2024), pp. 1950–1988. DOI: 10.1109/COMST.2024.3388511.

[6] CPRI Cooperation. *eCPRI Transpot Requirements V1.2*. 2018. URL: http://www.cpri.info/spec.html.

[7] NTT Docomo. *5G Evolution and 6G*. 2023. URL: https://www.docomo.ne.jp/english/corporate/technology/whitepaper_6g/.

[8] "IEEE Standard for Local and metropolitan area networks – Time-Sensitive Networking for Fronthaul". In: *IEEE Std 802.1CM-2018* (2018), pp. 1–62. DOI: 10.1109/IEEESTD.2018.8376066.

[9] ITU-T. *G.652 Characteristics of a single-mode optical fibre and cable*. 2024.

[10] ITU-T. *G.694.1 Spectral grids for WDM applications: DWDM frequency grid*. 2012.

[11] ITU-T. *G.698.5 Multichannel DWDM applications with single-channel optical interfaces in the O-band*. 2024.

[12] ITU-T. *G.698.6 Multichannel WDM applications with single-channel optical interfaces in the O-band*. 2024.

[13] Joonyoung Kim, Sun Hyok Chang, and Joon Ki Lee. "Comparative study for evaluating the cost efficiency of 5G Ethernet mobile fronthaul networks". In: *Journal of Optical Communications and Networking* 14.12 (2022), pp. 960–969. DOI: 10.1364/JOCN.471194.

[14] Daewon Lee et al. "Coordinated multipoint transmission and reception in LTE-advanced: deployment scenarios and operational challenges". In: *IEEE Communications Magazine* 50.2 (2012), pp. 148–155. DOI: 10.1109/MCOM.2012.6146494.

[15] Siva Muruganathan et al. "On the System-Level Performance of Coordinated Multi-Point Transmission Schemes in 5G NR Deployment Scenarios". In: *2019 IEEE 90th Vehicular Technology Conference (VTC2019-Fall)*. 2019, pp. 1–5. DOI: 10.1109/VTCFall.2019.8891098.

[16] Francesco Musumeci et al. "Optimal BBU Placement for 5G C-RAN Deployment Over WDM Aggregation Networks". In: *Journal of Lightwave Technology* 34.8 (2016), pp. 1963–1970. DOI: 10.1109/JLT.2015.2513101.

[17] O-RAN Alliance. *Open Xhaul Transport Working Group 9 - Xhaul Transport Requirements v01.00*. 2021. URL: https://o-ran.org/specifications.

[18] Cunhua Pan et al. "The Non-Coherent Ultra-Dense C-RAN Is Capable of Outperforming Its Coherent Counterpart at a Limited Fronthaul Capacity". In: *IEEE Journal on Selected Areas in Communications* 36.11 (2018), pp. 2549–2560. DOI: 10.1109/JSAC.2018.2874138.

[19] Neil Parkin et al. "eCPRI Radio Access Network Fronthaul Physical Reach Increase by using Hollow Core Fibre". In: *2021 European Conference on Optical Communication (ECOC)*. 2021, pp. 1–3. DOI: 10.1109/ECOC52684.2021.9605976.

[20] Rafael Puerta et al. "Experimental Validation of Coherent Joint Transmission in a Distributed-MIMO System with Analog Fronthaul for 6G". In: *2023 Joint European Conference on Networks and Communications and 6G Summit (EuCNC/6G Summit)*. 2023, pp. 585–590. DOI: 10.1109/EuCNC/6GSummit58263.2023.10188222.

[21] Cheng-Xiang Wang et al. "On the Road to 6G: Visions, Requirements, Key Technologies, and Testbeds". In: *IEEE Communications Surveys and Tutorials* 25.2 (2023), pp. 905–974. DOI: 10.1109/COMST.2023.3249835.

[22] Shangbin Wu and Yinan Qi. "Centralized and Distributed Schedulers for Non-Coherent Joint Transmission". In: *2018 IEEE Globecom Workshops (GC Wkshps)*. 2018, pp. 1–6. DOI: 10.1109/GLOCOMW.2018.8644228.

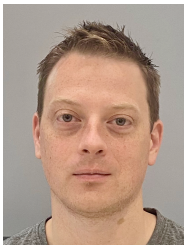

Dave Townend received the M.Eng degree in wireless communication engineering from Loughborough University, U.K., in 2007 and Ph.D in electronic systems engineering from the University of Essex, U.K., in 2024. He is currently a Wireless Research Manager at BT Laboratories and is a Chartered Engineer and a Member of the IET. His research interests include high frequency propagation, mobile network deployment modeling, transport network architecture and wireless backhaul.

Stuart D. Walker received the B.Sc. (Hons) degree in physics from Manchester University, U.K., in 1973, the M.Sc. degree in telecommunications systems and Ph.D. degree in electronics from Essex University, Colchester, U.K., in 1975 and 1981 respectively. From 1981-82, he was a post-doctoral research assistant at Essex University. From 1982-87, he was a research scientist at BT Laboratories, and from 1987-88 he was promoted to Group Leader in Submarine Systems Design. He joined Essex University in 1988 as a Senior Lecturer, and was promoted to Reader in 2002 and to Full Professor in 2004. At Essex University, he manages a laboratory concerned with all aspects of Access Networks: The Access Networks Group (ANG).

Neil Parkin received the M.Eng degree in electronic and optoelectronic engineering from the University of Hull, UK. He worked on optical transceiver design at Agilent Technologies until 2005. After a short time at Toshiba, he joined BT initially designing DWDM networks and then moving into research in 2012. He is currently an Optical Research Manager with research interests in optical fibers, sensing, and access networks.

Anvar Tukmanov is a radio communication systems engineer. He received the B.Eng. degree in mobile communications from Kazan National Research Technical University, named after A.N.Tupolev, Russia, in 2007. He received his M.Sc. and Ph.D. in electrical engineering from Newcastle University, U.K., in 2009 and 2015, respectively. Anvar is currently the Head of Wireless Research at BT Labs, focusing on fundamental and emerging technologies increasing spectral and energy efficiency, and architectural flexibility of Radio Access Networks. Prior to that Anvar led research in MIMO communication systems applied to LTE and NR air interface technologies. He has been representing BT at 3GPP RAN1 working group since 2015. He is a recipient of the 2020 UKRI Future Leaders Fellowship and is a Distinguished Engineer at BT.